Adaptive Cascade Hybrid Configurations for Linear Array Beamforming

Walter Orozco-Tupacyupanqui, Mariko Nakano-Miyatake and Hector Perez-Meana

Abstract— This paper presents the analysis of three proposed Least Recursive Mean Square (LRMS) hybrid cascade configurations for beamforming based on the Least Mean Square (LMS) and the Recursive Least Square (RLS) algorithm. It involves the use of the former single algorithm as a pre-filter and the latter one as a post-filter stage. Furthermore, the steering vector of the linear array is used as the interface between these two adaptive filters to form the hybrid cascade structure and generate the impinging signal to the post-filter block. The mathematical analysis of these new schemes is based on the orthogonality principle to prove the convergence to the optimal Wiener solution. Computer simulations have been performed to show the validity, reliability and limitations that these structures have in their capacity of recovering the desired signal corrupted by noise. In addition, the speed of these configurations is determined by the number of required iterations to reach the minimum square value of the learning curve.

Keywords— Adaptive antenna array, beamforming, cascade algorithms, LMS algorithm, RLS algorithm.

I. INTRODUCTION

NOWADAYS, there is an important further increase in the services provided by modern wireless communication systems. Common examples of these wireless equipment in use today include: telemetry control, infrared and ultrasonic remote control devices, specialized mobile radio (SMR) typically used by business, industrial and public safety entities, radio navigation equipment used by aviators and air traffic control, global positioning system (GPS), and of course cellular telephones and pagers with connectivity for portable and mobile applications, both personal and business. It is therefore not surprising that, the demand for a wider coverage, greater capacity and especially for a higher data rate is growing faster than ever due to the development of several applications for this type of systems. As a consequence of this growth, the possibility of having a larger number of interferences is inevitable.

For this reason, adaptive arrays and adaptive algorithms are currently the subject of extensive investigation as a mean for reducing the vulnerability of the reception of desired signals to presence of noise from the environment or interferences, undesired signals, from other sources in communication systems.

The concept of smart antennas implies the fact of the weights can be made adaptive, therefore a set of adaptive array processors filter the signals coming from the array, and direct the beam to several different directions where a communication is required. In general, this is a direct way to enhance the capacity of coverage and any adaptive communication system must be able to form a beam for each user according to its position. The capacity of these antennas to track their target signals hastily and precisely depends mainly on the performance of the beamforming algorithm employed [1]-[4].

Recently, variants of LMS and RLS hybrid algorithms have been investigated to enhance the convergence and tracking ability in beamforming systems. In [5], the authors propose and analyze a configuration, called RLMS; this hybrid system presents a flexible method of achieving either fixed or self-adaptive antenna beamforming. The convergence of RLMS is shown to be quite insensitive to variations in SNR of the input signal as well as the step sizes associated with the RLS and LMS sections.

In [6], a new adaptive algorithm, called least mean square-least mean square (LLMS) algorithm employs an array image factor, sandwiched in between two least mean square (LMS) algorithm sections. Unlike earlier LMS algorithm based techniques, this algorithm derives its overall error signal by feeding back the error signal from the second LMS algorithm stage to combine with that of the first LMS algorithm section. The fidelity of the signal at the output of an LLMS algorithm beamformer is demonstrated by means of the resultant values of error vector magnitude (EVM) and scatter plots.

Other adaptive cascade structures have been developed for different applications, for example in [7] the background noise recorded by microphones in a car environment is mainly caused by the engine, airflow and the tires. The engine noise can be suppressed by adaptive filtering where the filter consists of cascaded time-domain least mean squares (LMS) filters. Cascading the LMS filters improves the filter adaptation of the higher order harmonics.

This paper examines three different ways of forming hybrid cascade structures based on the internal programming of their adaptive algorithms, whether or not exist dependence between their errors signals and the manner in which the single LMS and RLS algorithms process information.

W. Orozco is enrolled in the Graduate PhD. program in Communications and Electronic Engineering, National Polytechnic Institute, Mexico City, Mexico (e-mail: waltozco@yahoo.com).

M. Nakano is with the Graduate studies and Research section of The Mechanical and Electrical Engineering School, National Polytechnic Institute Mexico City, Mexico (e-mail: mnakano@ipn.mx).

H. Perez Meana is with the Graduate studies and Research section of The Mechanical and Electrical Engineering School, National Polytechnic Institute Mexico City, Mexico (e-mail: hmperezm@ipn.mx).

For the first two configurations the same cascade structure has been used, but for the first system each adaptive algorithm works independently of each other in the sense of neither the pre-filer block nor the post-filter stage require the same number of iterations to reach the optimal weight values and the minimum square. However, the second block does not process any signal until the first block has performed all necessary iterations to reach its optimal conditions. The second hybrid model diverges from the first one in the fact of both algorithms work at the same time, thus both adaptive filters require the same number of iterations to reach the mean square error. Finally, the third configuration has a similar behavior to the second one, but the main difference lies in the fact that both algorithms depend on the same error generated by the RLS block, we recall that for the other two hybrid schemes, each sub-filter has their own error signal.

The rest of the paper is organized as follows. In Section III, computer simulations have been performed to compare the convergence and speed of these configurations and their capacity of recovering the desired signal corrupted by noise. Finally, Section IV concludes the paper.

II. CASCADE HYBRID STRUCTURES

A. Cascade Hybrid Independent Structure

Fig.1 shows the block diagram of a basic N-isotropic element linear array, assumed uniformly spaced, for beamforming, [8].
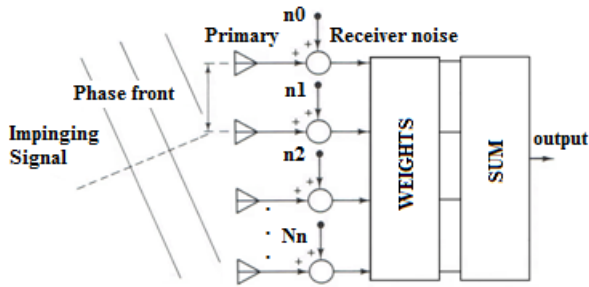
Fig.1 Arrangement of a linear array of N- isotropic elements

Let assume for the smart antenna system that the incoming signal has been corrupted by Additive White Gaussian Noise (AWGN), η of variance σ^2. For this type of systems the incident signal is first converted to baseband; therefore the carrier component is removed. In this way, the signals plus noise received by the antennas can be assumed to be of the form [9]-[11].

$$\mathbf{X} = s(t)\begin{bmatrix} 1 \\ e^{j2\pi d \cos\phi/(\lambda)} \\ e^{j4\pi d \cos\phi/(\lambda)} \\ \vdots \\ e^{j\pi(N-1)d \cos\phi/(\lambda)} \end{bmatrix} + \begin{bmatrix} \eta_o(t) \\ \eta_1(t) \\ \eta_2(t) \\ \vdots \\ \eta_{N-1}(t) \end{bmatrix} \quad (1)$$

$$\mathbf{X} = \sum_{n=0}^{N-1} s(t)e^{j2\pi nd \cos\phi/(\lambda)} + \eta \quad \text{for} \quad n = 0,1,\ldots N-1 \quad (2)$$

$$\mathbf{X} = s(t)\mathbf{F} + \eta \quad (3)$$

where $\mathbf{F}$ is known as the array factor or steering vector, ϕ is the arriving angle of the impinging signal, d is de the antenna element spacing, λ is the carrier signal, η is the noise vector, and $s(t)$ is the baseband signal or the envelope.

Fig.2 shows the block diagram of an N-isotropic element adaptive linear array, which employs first a LMS block as a pre-filter followed by a transversal adaptive RLS filter as its beamformer. According to Fig.2, the input stage of the hybrid scheme is based on the LMS algorithm whose weight vector is updated according to [9], [10]

$$\min_w E|y - xw|^2 \quad (4)$$

$$w_i = w_{i-1} + \mu x_i^*[y(i) - x_i w_{i-1}], \quad i \geq 0, \quad w_{-1} = \text{initial guess} \quad (5)$$

where the step-size μ is usually a small positive constant. On the other hand, the optimal weight vector that solves (4) for the second stage can be obtained recursively by the RLS algorithm as follows [9], [10]

$$P_i = \lambda^{-1}\left[P_{i-1} \frac{\lambda^{-1}P_{i-1}x_i^* x_i P_{i-1}}{1 + \lambda^{-1}x_i P_{i-1}x_i^*} \right] \quad (6)$$

$$w_i = w_{i-1} + P_i x_i^*[y(i) - x_i w_{i-1}] \quad (7)$$

with initial condition $P_{-1} = \epsilon^{-1}I$ for some small positive scalar ϵ where the forgetting factor is $0 \ll \lambda \leq 1$.

The analysis of the adaptive filter is developed by considering the adaptive linear combiner used for both stages in Fig.2. Now, after all iterations have been performed by the LMS algorithm, its output can be written as

$$y_{LMS} = \mathbf{W}_{LMS}^H \mathbf{X}_{LMS} = \mathbf{X}_{LMS}^H \mathbf{W}_{LMS} \quad (8)$$

The operator $\{\cdot\}^H$ represents Hermitian transpose [6], and bold letters denote matrices and vectors.

To obtain a fixed beam pointing to the direction of the required angle of arrival at the output of the second block, it is enough to multiply the output of the first block by the steering vector $\mathbf{F}$ [11]. Therefore, the input signal vector for the RLS stage can be obtained by

$$\mathbf{X}_{RLS} = \mathbf{F}y_{LMS} \quad (9)$$

By substituting (8) in (9) yields

$$\mathbf{X}_{RLS} = \mathbf{F}\mathbf{X}_{LMS}^H \mathbf{W}_{LMS} \quad (10)$$
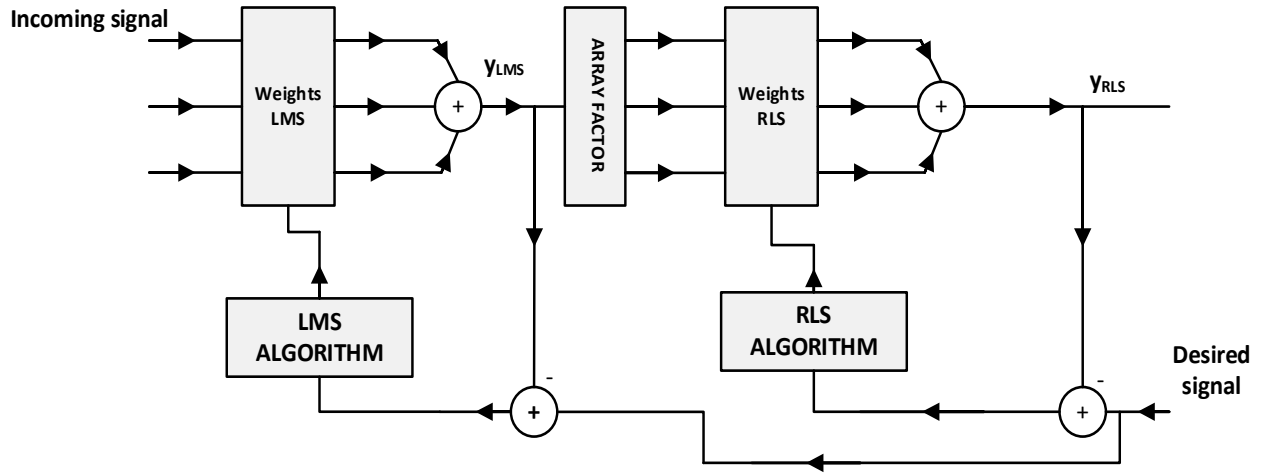
Fig.2 Cascade Hybrid Independent Structure

Finally, the output of the RLS block can be expressed as

$$y_{RLS} = \mathbf{W}_{RLS}^H \mathbf{X}_{RLS} = \mathbf{X}_{RLS}^H \mathbf{W}_{RLS} \qquad (11)$$

$$y_{RLS} = \mathbf{W}_{RLS}^H \mathbf{F} \mathbf{W}_{LMS}^H \mathbf{X}_{LMS} \qquad (12)$$

$$y_{RLS} = \mathbf{W}_{LRMS}^H \mathbf{X}_{LMS} \qquad (13)$$

To minimize the mean-square errors $E\{e_{LMS}^2\}$ and $E\{e_{RLS}^2\}$, the orthogonality principle [11]-[13] in MSE estimation is used, according to which the optimum weight vector is obtained from the condition that the input vector is orthogonal to the error signal. Thus, the optimization of the weights of the first block can be calculated by

$$E\{e_{LMS}\mathbf{X}_{LMS}\} = 0 \qquad (14)$$

$$E\{(d - y_{LMS})\mathbf{X}_{LMS}\} = 0 \qquad (15)$$

$$E\{d\mathbf{X}_{LMS}\} - E\{\mathbf{X}_{LMS} y_{LMS}\} = 0 \qquad (16)$$

By substituting (8) into the second term of the RHS of (16) yields

$$E\{d\mathbf{X}_{LMS}\} - E\{\mathbf{X}_{LMS}\mathbf{X}_{LMS}^H \mathbf{W}_{LMS}^*\} = 0 \qquad (17)$$

$$E\{d\mathbf{X}_{LMS}\} - E\{\mathbf{X}_{LMS}\mathbf{X}_{LMS}^H\}\mathbf{W}_{LMS}^* = 0 \qquad (18)$$

The operator $\{\cdot\}^*$ represents the optimal value of the weights for the transversal filter [9].

The first term of the RHS is the cross correlation column vector $\mathbf{P}$ between the desired signal d and the input vector $\mathbf{X}$, and the second term is the input correlation matrix $\mathbf{R}$ [9]. Finally, from (18) the optimal LMS weights can be obtained by

$$\mathbf{P}_{LMS} - \mathbf{R}\mathbf{W}_{LMS}^* = 0 \qquad (19)$$

$$\mathbf{W}_{LMS}^* = (\mathbf{R}_{LMS})^{-1}\mathbf{P}_{LMS} \qquad (20)$$

Now, the optimization of the weights for the second block follows a similar procedure, thus

$$E\{e_{RLS}\mathbf{X}_{RLS}\} = 0 \qquad (21)$$

$$E\{(d - y_{RLS})\mathbf{X}_{RLS}\} = 0 \qquad (22)$$

$$E\{d\mathbf{X}_{RLS}\} - E\{\mathbf{X}_{RLS} y_{RLS}\} = 0 \qquad (23)$$

By substituting (8) and (9) in the first RHS term of (23) yields

$$E\{d\mathbf{X}_{RLS}\} = E\{dy_{LMS}\mathbf{F}\} \qquad (24)$$

$$E\{d\mathbf{X}_{RLS}\} = E\{d\mathbf{X}_{LMS}^H\}\mathbf{W}_{LMS}^*\mathbf{F} \qquad (25)$$

$$E\{d\mathbf{X}_{RLS}\} = \mathbf{P}_{LMS}^H \mathbf{W}_{LMS}^*\mathbf{F} \qquad (26)$$

Now, by substituting (13) in the second RHS term of (23) yields

$$E\{\mathbf{X}_{RLS} y_{RLS}\} = E\{\mathbf{X}_{RLS}\mathbf{X}_{RLS}^H \mathbf{W}_{RLS}^*\} \qquad (27)$$

$$= \mathbf{F}\mathbf{W}_{LMS}^{*H} E\{\mathbf{X}_{LMS}\mathbf{X}_{LMS}^H\}\mathbf{W}_{LMS}^*\mathbf{F}^H \mathbf{W}_{RLS}^* \qquad (28)$$

$$= \mathbf{F}\mathbf{W}_{LMS}^{*H}\mathbf{R}_{LMS}\mathbf{W}_{LMS}^*\mathbf{F}^H \mathbf{W}_{RLS}^* \qquad (29)$$

Finally, the optimal weights for the RLS stage can be obtained by substituting (26) and (29) in (23), therefore

$$\mathbf{W}_{RLS}^{*} = \left(\mathbf{F}\mathbf{W}_{LMS}^{*H}\mathbf{R}_{LMS}\mathbf{W}_{LMS}^{*}\mathbf{F}^{H}\right)^{-1}\mathbf{P}_{LMS}^{H}\mathbf{W}_{LMS}^{*}\mathbf{F} \qquad (30)$$

In order to rewrite (30) in a more compact form, a new correlation matrix and cross correlation vector are defined for the second stage as follow

$$\overset{\Delta}{\mathbf{R}}_{RLS} = \mathbf{F}\mathbf{W}_{LMS}^{*H}\mathbf{R}_{LMS}\mathbf{W}_{LMS}^{*}\mathbf{F}^{H} \qquad (31)$$

$$\overset{\Delta}{\mathbf{P}}_{RLS} = \mathbf{P}_{LMS}^{H}\mathbf{W}_{LMS}^{*}\mathbf{F} \qquad (32)$$

Finally, (30) can be written as

$$\mathbf{W}_{RLS}^{*} = (\overset{\Delta}{\mathbf{R}}_{RLS})^{-1}\overset{\Delta}{\mathbf{P}}_{RLS} \qquad (33)$$

According to (33) the optimal weights of the second beamforming block depend on the optimal values of the first block after this one performed all necessarily iterations to reach convergence to its optimal weights. In addition, both (20) and (33) converge to the Wiener weight vector solution [14].

Fig.3 shows the flow diagram of the programming structure of these blocks which indicates that each stage is independent of the other one in the sense of they do not belong to the same closed loop, as a consequence of this each algorithm does not necessarily require the same number of iterations to reach the optimal weight values.
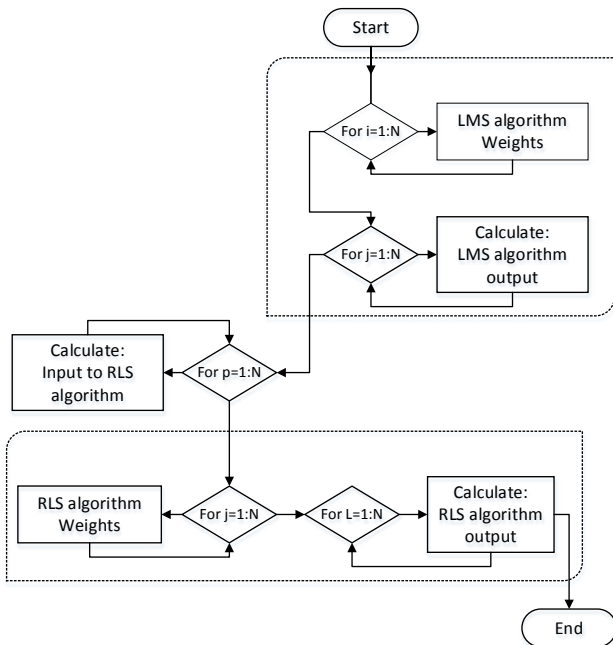
Fig.3 The flow diagram of the LRMS algorithm for independent blocks

B. Cascade Hybrid not Independent Structure

The scheme used for this hybrid structure is the same structure shown in Fig.2, but the essential difference lies on the fact that both algorithms work under the same closed loop

as shown in Fig.4.

For this second hybrid scheme, (20) and (33) rule its behavior, but both equations are updated at the same time by (5), (6) and (7) until to converge to the optimal weight instead of waiting the LMS algorithm first executes all iterations.
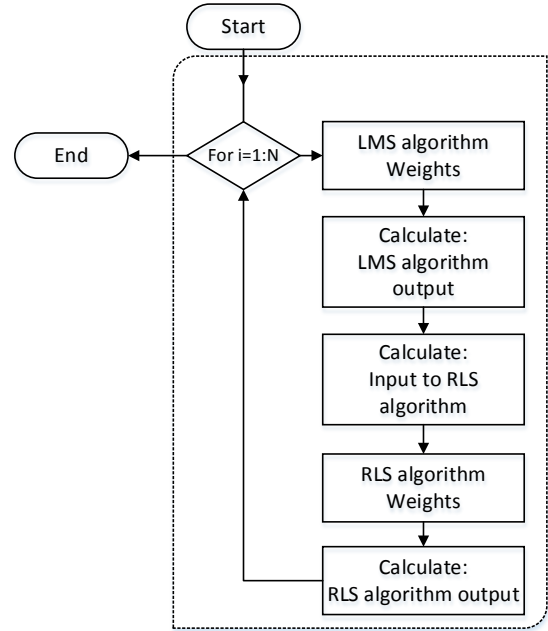
Fig.4. The flow diagram of the LRMS algorithm for not independent blocks

C. Cascade Hybrid not Independent Structure with a Common Signal Error

Fig.5 shows the configuration of this third scheme. In this particular structure both algorithms work under the same error signal which has been taken from the RLS block due to this is the main beam former in this hybrid scheme.

Even though, the LMS block does not have an error signal by itself, the optimal values of its weights can be obtained by using the RLS block error, therefore

$$E\{e_{RLS}\mathbf{X}_{LMS}\} = 0 \qquad (34)$$

$$E\{(d - y_{RLS})\mathbf{X}_{LMS}\} = 0 \qquad (35)$$

$$E\{d\mathbf{X}_{LMS}\} - E\{\mathbf{X}_{LMS}y_{RLS}\} = 0 \qquad (36)$$

The first term of the RHS is only the cross correlation column vector $\mathbf{P}_{LMS}$ and the output of the RLS block is $y_{RLS} = \mathbf{X}_{RLS}^{H}\mathbf{W}_{RLS}$, therefore (36) can be written as

$$\mathbf{P}_{LMS} - E\{\mathbf{X}_{LMS}\mathbf{X}_{RLS}^{H}\mathbf{W}_{RLS}^{*}\} = 0 \qquad (37)$$

By substituting (8) and (9) in (37), and after some straight forward manipulation, we have

$$\mathbf{P}_{LMS} - E\{\mathbf{X}_{LMS}\cdot\mathbf{X}_{LMS}^{H}\}\mathbf{W}_{LMS}^{*}\mathbf{F}^{H}\cdot\mathbf{W}_{RLS}^{*} = 0 \qquad (38)$$
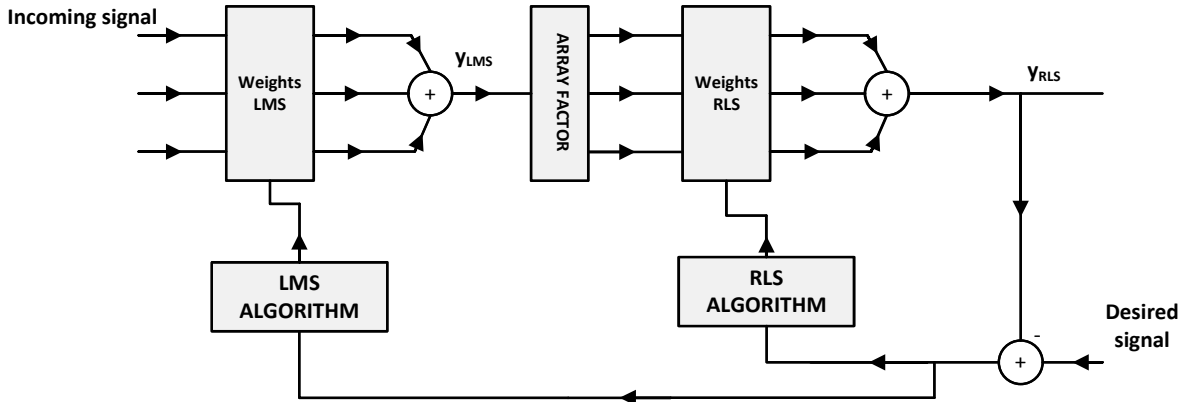
Fig.5. The LRMS configuration for not independent blocks with a common error

$$\mathbf{W}^*_{LMS} = \mathbf{R}^{-1}_{LMS} \mathbf{P}_{LMS} \left(\mathbf{F}^H \mathbf{W}^*_{RLS} \right)^{-1} \qquad (39)$$

A new cross correlation vector is defined for the second stage as follow

$$\overset{\Lambda}{\mathbf{P}}_{LMS} = \mathbf{P}_{LMS} \left(\mathbf{F}^H \mathbf{W}^*_{RLS} \right)^{-1} \qquad (40)$$

Finally, (40) can be written as

$$\mathbf{W}^*_{LMS} = \mathbf{R}^{-1}_{LMS} \overset{\Lambda}{\mathbf{P}}_{LMS} \qquad (41)$$

Equation (41) converges to the Wiener solution [10] and depends on the optimal value of the RLS weights. However, at the first iteration the value of W_{RLS} is calculated by its algorithm before the LMS weight, and once the corresponding error has been calculated this can be used to calculate the consequent W_{LMS} as shown in Fig.6. Therefore, (5) must be written as

$$w_{LMS(i)} = w_{LMS(i-1)} + \mu x^H_i e_{RLS(i-1)}, \quad i \geq 2, \qquad (42)$$

In addition, for this hybrid scheme (33) is still ruling the behavior of the second stage, even though the internal programming has been changed due to the common error signal generated in the RLS block for both algorithms.

III. COMPUTER SIMULATIONS

The ability of the three cascade hybrid schemes to recover the transmitted signal corrupted by AWG noise is investigated by mean of MATLAB® simulations. For comparison purposes, results have also been obtained for single LMS and RLS algorithms. For the simulation, the following parameters have been used:

- Two linear arrays of 4 and 20 isotropic antenna elements spaced quarter wavelength apart.
- The desired signal arrives at 60° degrees.

- The variance of the noise has been increased from 0.1 to 0.9.
- All weight vectors are initially set to zero for the adaptive algorithms.
- Each simulation run involves 300 samples.
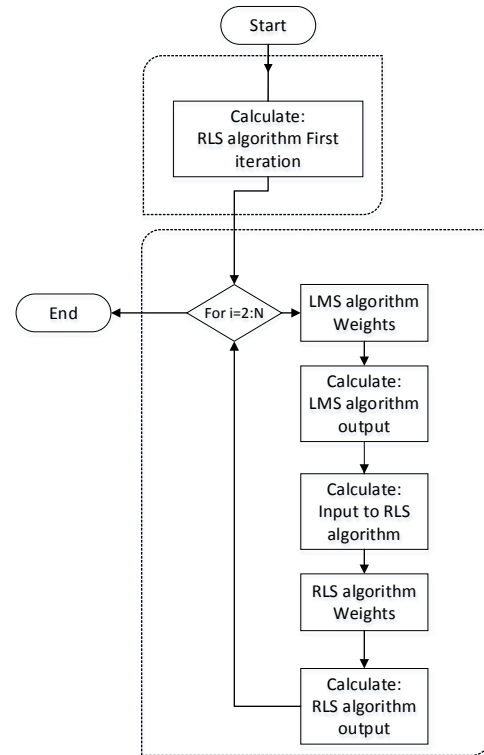
Fig.6 The flow diagram of proposed LRMS algorithm for not independent block with previous stage

Fig.7 shows the baseband signal corrupted by Additive Gaussian Noise (AWGN) at first four antennas for both linear arrays. In this case the noise signal at each antenna is white with real and imaginary components with variance of 0.1. In addition, the noise signals across the antennas are uncorrelated to each other.
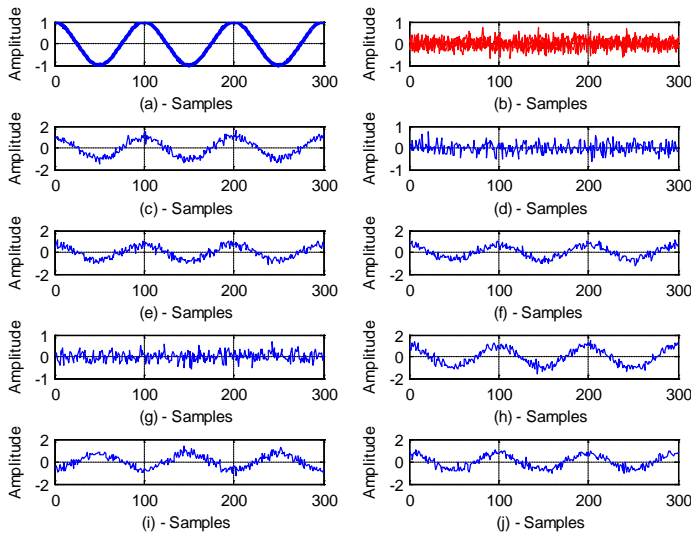
Fig.7 (a) Baseband signal, (b) AWGN with $\sigma_n^2 = 0.1$, (c) - (j) the real and complex components at first four antennas for the linear array of 4 and 20 isotropic antenna elements, respectively.
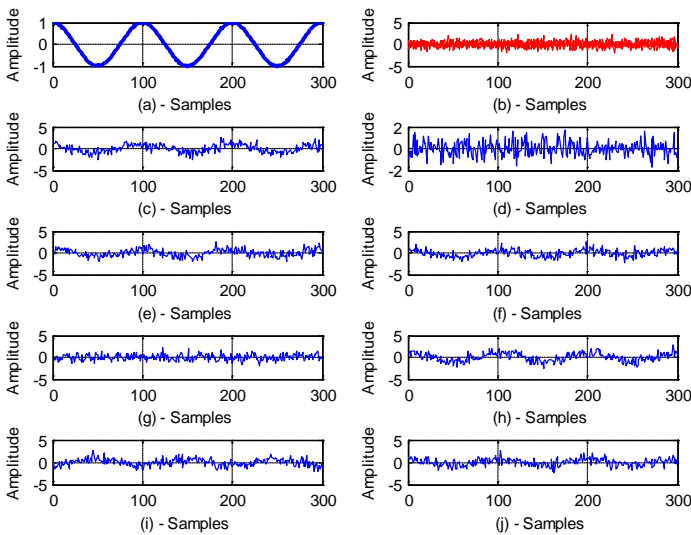
Fig.8 (a) Baseband signal, (b) AWGN with $\sigma_n^2 = 0.9$, (c) – (j) the real and complex components at first four antennas for the linear array of 4 and 20 isotropic antenna elements, respectively.

Fig.8 shows the same baseband signal coming to the linear array as in Fig.7, except that the noise variance has been increased to 0.9 to simulate a worst interference. It is important to recall that the transmitted signal does not have any imaginary component; however, it has been separated into two components due to the array factor. Fig.9 shows the recovered signals after applying the optimal weights obtained by the first hybrid scheme. For this simulation the noise variance is 0.1 and the number of isotropic elements is four. According to the plots, the real component of the recovered signal is almost exactly in each sample of the transmitted signal. On the other hand, the imaginary components present some dispersion around the transmitted imaginary component which actually is zero. Nevertheless, its magnitude is around ±0.05, thus it could almost be considered as zero.
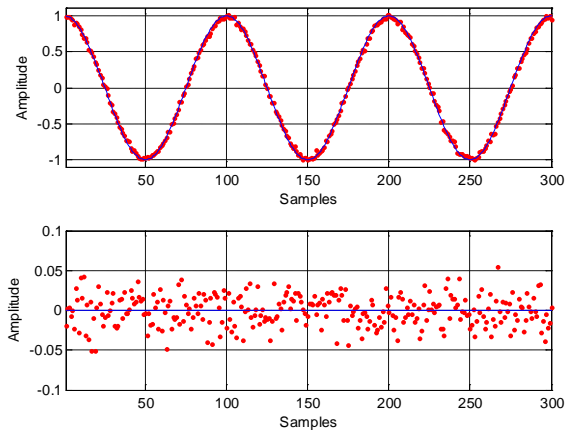
Fig.9 Transmitted signal (solid line) and recovered signal (spot line) for the real and complex components at the output of the beamforming for the four linear array. AWGN with $\sigma_n^2 = 0.1$. Cascade Hybrid Independent Structure

Similar solutions were obtained by the cascade hybrid not independent structure (CHNIS) and the cascade hybrid not independent structure with a common error (CHNISCE) at the output of the beamforming. Fig. 10 and Fig.11 show these results, respectively. However, according to Fig.11 the complex component of the recovered signal is similar to a sine wave with a small amplitude.
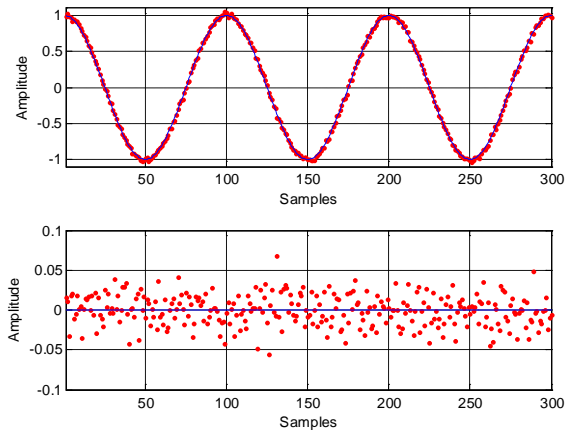
Fig.10 Transmitted signal (blue line) and recovered signal (red spots) for the real and complex components at the output of the beamforming for the four linear array. AWGN with $\sigma_n^2 = 0.1$. Cascade Hybrid not Independent Structure

Fig.12, Fig. 13 and Fig. 14 show the recovered signals after applying the optimal weights obtained by the three hybrid algorithms, respectively. For this experiment, 16 isotropic elements were added to the primer antenna array. For this system the noise variance is still 0.1. As a result of having a larger number of elements in the arrangement, twenty elements, more samples of the impinging signal for the adaptive filter can be obtained for estimation; as a consequence the real component of the estimated signal is almost exact to the desired information signal, whereas the complex red spots are scattered in the range of ±0.02 instead of ±0.05.
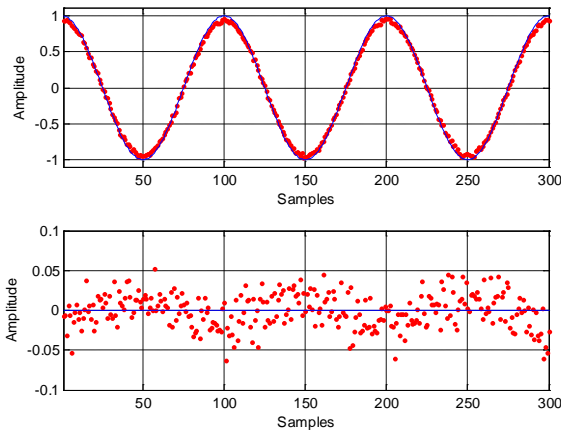
Fig.11 Transmitted signal (blue line) and recovered signal (red spots) for the real and complex components at the output of the beamforming for the four linear array. AWGN with $\sigma_n^2 = 0.1$. Cascade Hybrid not Independent Structure

Fig.12 Transmitted signal (solid line) and recovered signal (spot line) for the real and complex components at the output of the beamforming for the twenty linear array. AWGN with $\sigma_n^2 = 0.1$. Cascade Hybrid Independent Structure

Fig.13 Transmitted signal (solid line) and recovered signal (spot line) for the real and complex components at the output of the beamforming for the twenty linear array. AWGN with $\sigma_n^2 = 0.1$. Cascade Hybrid not Independent Structure
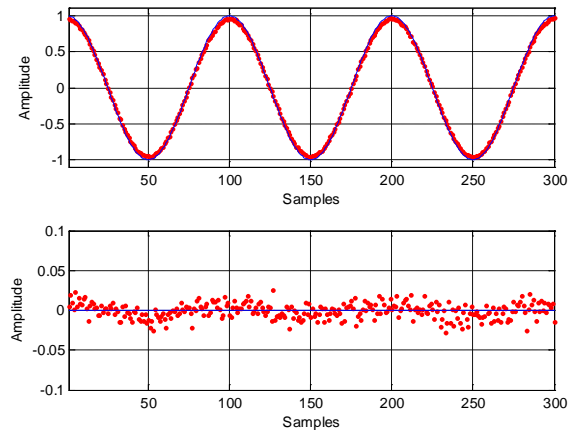
Fig.14 Transmitted signal (solid line) and recovered signal (spot line) for the real and complex components at the output of the beamforming for the twenty linear array. AWGN with $\sigma_n^2 = 0.1$. Cascade Hybrid not Independent Structure with a Common Signal Error.
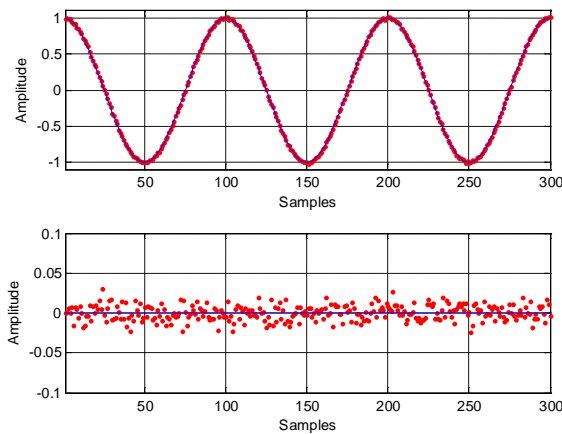
Fig.15 shows the recovered signals for the first scheme after the noise variance has been increased to 0.9 for the four linear antenna array. Due to the worst condition, the capability of recovering the real component is significantly reduced; however, it is still possible to identify the estimated information signal. The worst result is in regard to the imaginary component, where the dispersion of the retrieved points is greater and their variation is around ±0.1.

On the contrary, Fig. 16 shows the recovered signal at the output of the adaptive beamformer for a twenty linear antenna array for the same noise variance of 0.9. In principle it is verified that the recovery of the information signal is still better for a linear array with a larger number of isotropic elements; however, the negative effects of increasing the noise condition are still visible in the signal recovery. For this case, the dispersion of the retrieved points is lesser and whose variation is around ±0.05. A similar behavior is displayed for the other two schemes for both conditions.
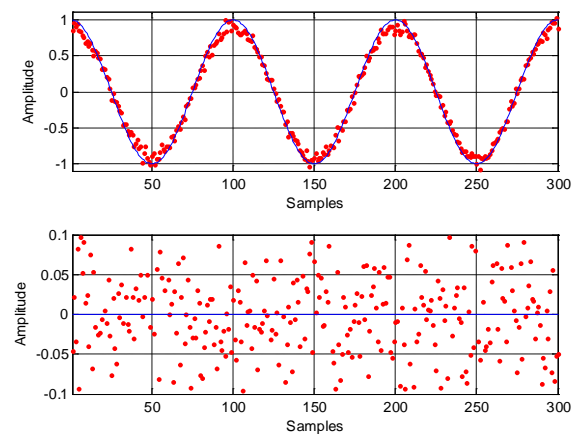
Fig.15 Transmitted signal (blue line) and recovered signal (red spots) for the real and complex components at the output of the beamforming for the four linear array, first scheme. Additive AWGN with $\sigma_n^2 = 0.9$
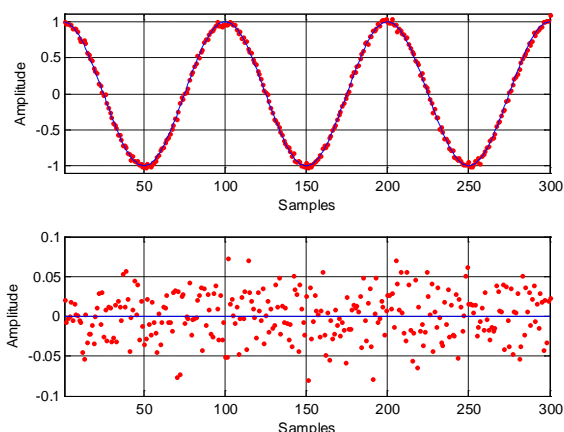
Fig.16 Transmitted signal (solid line) and recovered signal (spot line) for the real and complex components at the output of the beamforming for the 20 linear array, first scheme. AWGN with $\sigma_n^2 = 0.9$

Table I shows the mean square error between the real component of the desired signal and the signal recovered by the three hybrid architectures and two basic LMS and RLS algorithms, and Table II the complex components. One hundred individual simulations were performed and an ensemble average square error was calculated by (43).

$$mse = \left\| \hat{s}_i - s_i \right\|^2 / N \qquad (43)$$

The operator $\|\cdot\|$ represents the Euclidean norm [6] between the estimated signal and the information or desired signal, and N is the number of samples.

Table I. Mean Square Error vs. Noise Variance (0.1-0.9) – 4 Linear Array (Real Component) – Average.

	LMS	RLS	Arch.1	Arch.2	Arch.3
0.1	0.0127	0.0124	0.0128	0.0126	0.0316
0.2	0.0249	0.0246	0.0246	0.0263	0.0418
0.3	0.0367	0.0366	0.0371	0.0399	0.0513
0.4	0.0481	0.0474	0.0486	0.0539	0.0614
0.5	0.0599	0.0597	0.0577	0.0699	0.0889
0.6	0.0707	0.0696	0.0700	0.0844	0.0798
0.7	0.0807	0.0790	0.0786	0.0989	0.0943
0.8	0.0939	0.0908	0.0881	0.1166	0.0975
0.9	0.1035	0.1016	0.0988	0.1347	0.1056

Table II. Mean Square Error vs. Noise Variance (0.1-0.9) – 4 Linear Array (Imaginary Component) – Average.

	LMS	RLS	Arch.1	Arch.2	Arch.3
0.1	0.0122	0.0112	0.0127	0.0126	0.0174
0.2	0.0234	0.0206	0.0251	0.0261	0.0196
0.3	0.0341	0.0286	0.0355	0.0397	0.0376
0.4	0.0409	0.0349	0.0466	0.0531	0.0374
0.5	0.0521	0.0399	0.0553	0.0686	0.0757
0.6	0.0610	0.0447	0.0655	0.0835	0.0677
0.7	0.0679	0.0483	0.0734	0.0989	0.0506
0.8	0.0751	0.0518	0.0799	0.1157	0.0615
0.9	0.0811	0.0544	0.0886	0.1288	0.0856
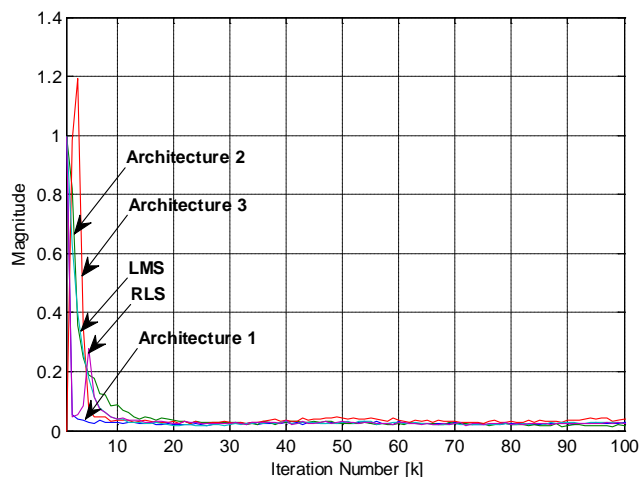
Fig.17 Average learning curves corresponding to the cases of an optimal constant step-size for the LMR, RLS and LMRS algorithms for the 4 linear array. Additive AWGN with $\sigma_n^2 = 0.1$
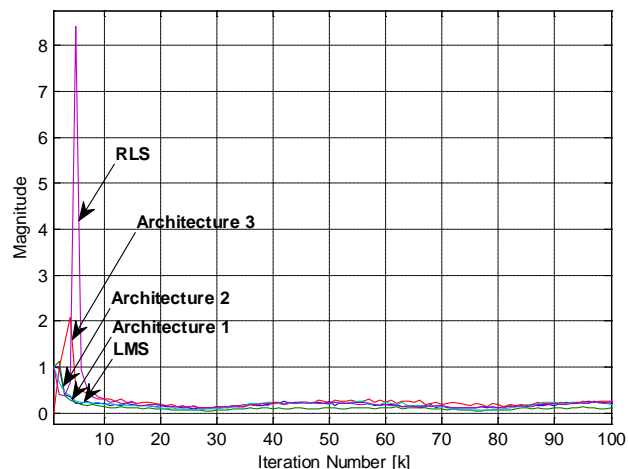
Fig.18 Average learning curves corresponding to the cases of an optimal constant step-size for the LMR, RLS and LMRS algorithms for the 4 linear array. Additive AWGN with $\sigma_n^2 = 0.9$

Fig.17 shows learning curves for the single LMS, RLS and LMRS algorithms for the first 100 iterations and a noise variance of 0.1. On the other hand, Fig.18 shows learning curves for the same algorithms, except that the noise variance has been increased to 0.9. According to Fig.17 when the characteristics of the noise are not severe, that is to say the variance is low. The cascade hybrid independent structure learns faster than the other four algorithms. It approximately requires 10 iterations on average in order to reach its minimum square error. On the other hand, the cascade hybrid not independent structure requires approximately 25 iterations, which make it the slowest algorithm for learning. We must recall that 100 individual simulations were performed in order to obtain these curves. Nevertheless, when the noise variance has been increased to 0.9, the learning curves of the two first hybrid configurations are similar to a single LMS algorithm, whereas the last hybrid configuration is similar to a single RLS algorithm as shown in Fig.18.

Owing to the four linear array is more susceptible to the

effects of noise, most of information in this paper is related to arrays whose number of antennas are enough to obtain a good estimation of the information signal, mean square error less than 0.01, but not enough to be considered as satisfactory. For example, the four linear array studied in this analysis. Table III shows the mean square error reached by the learning curves for the three hybrid architectures and two basic LMS and RLS algorithms.

Table III. Learning curve (Mean Square Error) vs. Noise Variance (0.1-0.9) – 4 Linear Array

	LMS	RLS	Arch.1	Arch.2	Arch.3
0.1	0.0248	0.0244	0.0228	0.0207	0.0355
0.2	0.0473	0.0458	0.0443	0.0351	0.0710
0.3	0.0677	0.0660	0.0616	0.0499	0.0905
0.4	0.0850	0.0830	0.0802	0.0587	0.1119
0.5	0.1022	0.1019	0.0920	0.0677	0.1252
0.6	0.1152	0.1152	0.1045	0.0714	0.1427
0.7	0.1322	0.1266	0.1149	0.0780	0.1603
0.8	0.1454	0.1433	0.1278	0.0836	0.1599
0.9	0.1627	0.1509	0.1393	0.0840	0.1790

For the hybrid algorithms, an adequate setting of the step-size and forgetting factor is considerably important. Fig.19, Fig.20 and Fig.21 show the mean square error obtained by five runs of each algorithm versus the increment of the noise variance, respectively. For the two first hybrid schemes the step-size μ was fixed on a value of 0.05±0.001. For these algorithms, there is not a significant difference among the mean square errors calculated for each run in each noise variance value. We only show the first five runs out of 100 that were performed because a similar behavior was visualized for the rest performances. In these Figs, it is possible to visualize almost a linear increment of this error according to the increment of the noise variance.
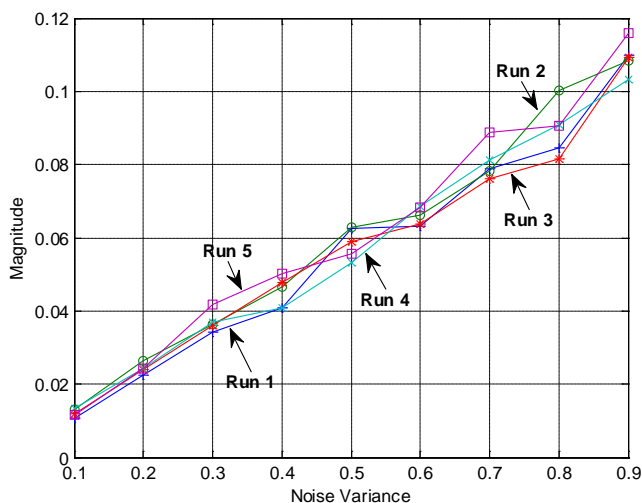
Fig.19. Mean square error curves corresponding to five runs of the Cascade Hybrid Independent Structure algorithm for an AWGN from $\sigma_n^2 = 0.1$ to $\sigma_n^2 = 0.9$, and $\mu = 0.05 \pm 0.001$.

In Fig.21, we observe that some of the mean square errors are not closed in magnitude for the same noise variance, even though the step-size and forgetting factor has been fixed for that condition.

Among the three proposed hybrid algorithms, the two first schemes are more robust than the third one with respect to the noise changes. Therefore, it was not required to make high modifications to the LMS step-size μ and the RLS forgetting factor λ. We could use almost the same parameters (μ and λ) for these two algorithms, even though the noise variance was increased.
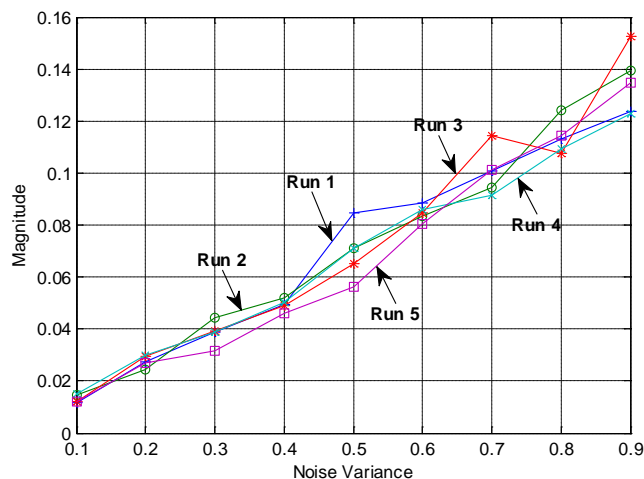
Fig.20. Mean square error curves corresponding to five runs of the Cascade Hybrid not Independent Structure algorithm for an AWGN from $\sigma_n^2 = 0.1$ to $\sigma_n^2 = 0.9$, and $\mu = 0.05 \pm 0.001$.

On the contrary, for the third hybrid algorithm was necessary to establish different value parameters for each increment of the noise variance. In fact, the use of a wrong step-size implies to have a recovered signal which is equal to the desired signal in phase and frequency, but with different amplitudes as shown in Fig.22. As a consequence, the estimated signal can be attenuated or amplified.
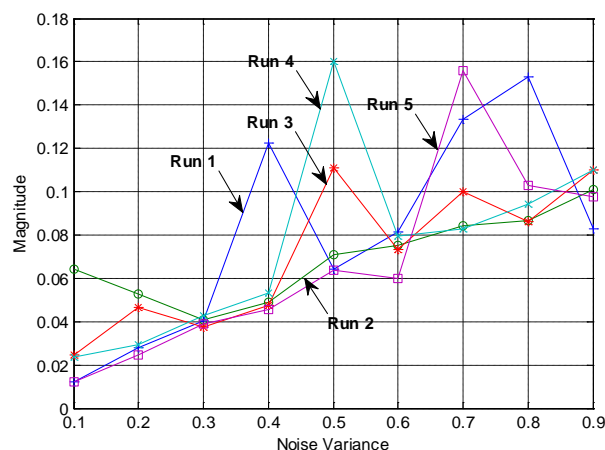
Fig.21. Mean square error curves corresponding to five runs of the Cascade Hybrid not Independent Structure with the same error algorithm for an AWGN from $\sigma_n^2 = 0.1$ to $\sigma_n^2 = 0.9$

The side lobe canceling effects are shown in Fig.23 and Fig.24, for the four and twenty linear array, respectively. Even though the effects of the noise are present, the three hybrid

schemas are able to generate a main lobe pointing to the desire angle of 60 degrees. In addition, the form of the beam pattern depends on the number of sensors, antennas or isotropic elements that compose the linear array.
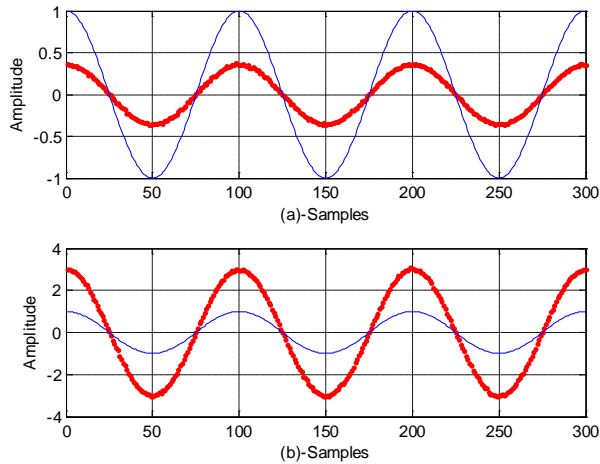
Fig.22. (a) Transmitted signal (blue line) and attenuated recovered signal (red spots) for the real component at the output of the beamforming for the four linear array, third scheme and wrong step-size μ. (b) Transmitted signal (blue line) and amplified recovered signal (red spots) for the real component at the output of the beamforming for the twenty linear array, third scheme and wrong step-size μ. Additive AWGN with $\sigma_n^2 = 0.1$.
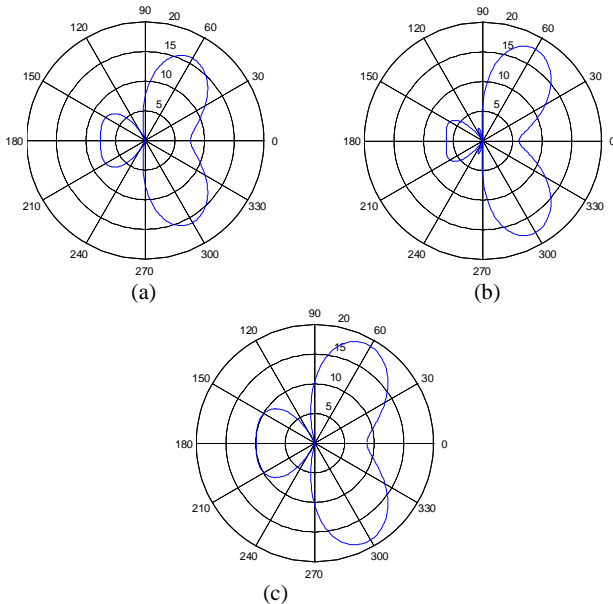
Fig.23 The Beam patterns for the hybrid schemes for the linear array of 4 isotropic antenna elements with additive AWGN with $\sigma_n^2 = 0.1$. (a) Cascade Hybrid Independent Structure (b) Cascade Hybrid not Independent Structure (c) Cascade Hybrid not Independent Structure with a common signal error.

Fig.25 shows the effects of noise on the output power generated by the beamformer. Although a main lobe was generated to the desired angle by the hybrid schemes, the output power decreases as the variance increases. Table IV shows in detail the power obtained by proposed schemes and the LMS and RLS algorithms for different noise conditions.
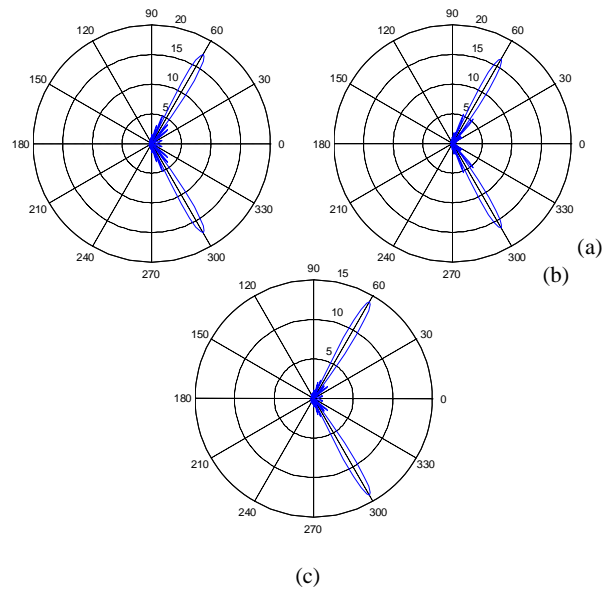
Fig.24 The Beam patterns for the hybrid schemes for the linear array of 20 isotropic antenna elements with additive AWGN with $\sigma_n^2 = 0.9$. (a) Cascade Hybrid Independent Structure (b) Cascade Hybrid not Independent Structure (c) Cascade Hybrid not Independent Structure with a common signal error.
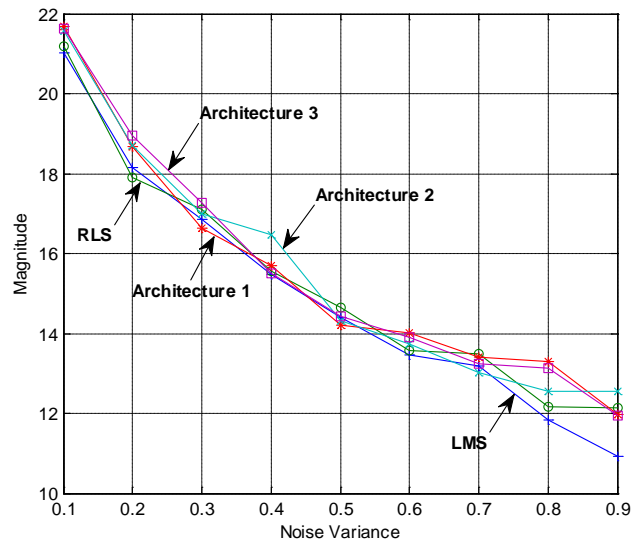
Fig.25 Output power (dB) versus noise variance from $\sigma_n^2 = 0.1$ to $\sigma_n^2 = 0.9$ for the 4 linear array.

According to Table IV the hybrid schemes were able to obtain a higher output power in seven out of nine cases. However, it is not possible to specify which one of the hybrid schemes is the best due to a permanent output power curve is not observed for each scheme. The cascade hybrid independent structure was able to generate the highest output power for $\sigma_\eta^2 = 0.1, 0.6$ and 0.8, the second algorithm for $\sigma_\eta^2 = 0.4$ and 0.9, finally the third schemes for $\sigma_\eta^2 = 0.2$ and 0.3. The rest highest results were obtained by the RLS algorithms and the worst results were calculated by the LMS algorithm.

Table IV. Output Power (dB) vs. Noise Variance (0.1-0.9) – 4 Linear Array.

	LMS	RLS	Arch.1	Arch.2	Arch.3
0.1	21.034	21.191	21.691	21.574	21.636
0.2	18.145	17.901	18.666	18.714	18.945
0.3	16.851	17.108	16.625	16.996	17.282
0.4	15.484	15.561	15.684	16.481	15.501
0.5	14.399	14.648	14.215	14.317	14.431
0.6	13.466	13.570	14.011	13.729	13.908
0.7	13.200	13.494	13.397	13.030	13.245
0.8	11.836	12.178	13.294	12.546	13.129
0.9	10.927	12.140	11.970	12.563	11.951

Fig.26 shows the convergence to the optimal solution of the real component of the first weight of the beamforming linear array of four isotropic elements with variance of 0.1. All algorithms have been considered for analysis. Comparing their curves, we note that the weight belonging to the cascade hybrid independent structure, LRMS(1), seems to converge more rapidly to the desired Wiener solution. On the contrary, the third hybrid scheme apparently is the slowest one.
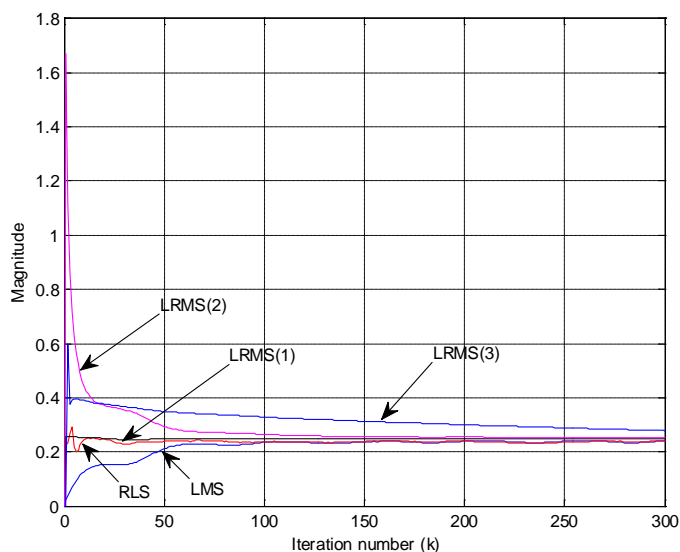
Fig.26 Convergence of the first weight to the Wiener solution for the single LMS, RLS and Hybrid algorithms. Real components for the four linear array. $\sigma_n^2 = 0.1$

Fig. 27 shows the convergence to the optimal solution of the imaginary component of the first weight. Even though, the first hybrid algorithm reached the optimal solution for the real component faster than the others, for the imaginary component the second scheme was more rapidly than the first hybrid algorithm. However, the number of iterations required for the second algorithm to reach the Wiener solution is almost imperceptible. A similar behavior was found for the other real and complex components of the weights for the four linear array system.

Other experiments were performed for this linear array, nevertheless similar convergence behavior were found for its weights when the noise variance was increased to $\sigma_\eta^2 = 0.9$.
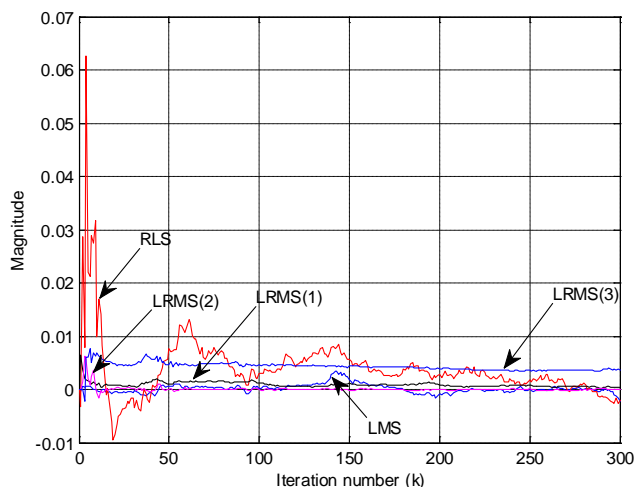
Fig.27 Convergence of the first weights to the Wiener solution for the single LMS, RLS and Hybrid algorithms. Imaginary components for the four linear array. $\sigma_n^2 = 0.1$

IV. CONCLUSIONS

Three proposed hybrid cascade LRMS algorithms have been investigated. The results show that all hybrid algorithms were able to obtain beam patterns pointing to the desired angle. It has also been proved by analytical analysis that all hybrid algorithms converge to the optimal Wiener solution.

In general, in most of the cases the learning curves of the hybrid configurations have a better convergence performance than the transversal single LMS and RLS filters. Moreover, the mean-square error does not increase its magnitudes, even though the number of stages is larger.

ACKNOWLEDGMENT

APPENDIX

The Matlab® programs for the single LMS and RLS algorithms used to generate the hybrid schemes are exposed in this Appendix.

Program.1: LMS algorithm.

```
% LMS Algorithm.
% N: Number of iterations.
% e: error
%wlms: LMS weights.
% u: step size
% d: desired signal
% H: incoming signal

1: for n=1:N
2:    e(n)=d(n)-H(n,:)*wlms;
3:    wlms=wlms+u*H(n,:)'*e(n);
4: end
```

Program.2: RLS algorithm.

```
% RLS Algorithm.
%N: Number of iterations.
% e: error
%wrls: RLS weights.
% lambda: forgetting factor.
% d: desired signal
% H: incoming signal
% P: Inverse regularization factor matrix.

1: for n=1:N
2:    e(n)=d(n)-H(n,:)*wrls;
3:    P=inv(lambda)*(P-((inv(lambda)*P*H(n;:)'*H(n,:)*P)
      /(1+inv(lambda)*H(n,:)*P*H(n,:) ')));
4:    wrls=wrls+P*H(n,:)'*e(n);
5: end
```

REFERENCES

[1] W. Orozco and H. Pérez, "Cascade Hybrid LRMS Adaptive Configurations for Linear Array Beamforming", Proceeding of the 13th International Conference on Applied Computer Science, pp. 66-71, Morioka City, Japan, April 2013.

[2] R. Wongsan, "A Wide Beam Array Antenna Using Short End Curved Dipoles on Reflector Planes" WSEAS Transaction on Communications Vol. 8, pp. 207-216, 2009

[3] M. Bank, S. Slupenko, M. Haridin and V. Tsingus, "Orthogonal MIMO Antennas for Compact Cellular Handsets", International Journal of Communications, Vol. 6, pp. 89-97, 2012.

[4] M. Popescu and N. Mastorakis, "New Aspects of Wireless Communications, Vol. 3, pp. 34-43, 2009.

[5] J. A. Srar and K.-S. Chung, "Adaptive RLMS Algorithm for Antenna Array Beamforming", TENCON 2009 - 2009 IEEE Region 10 Conference, pp. 1-6, Singapore, November 2009.

[6] J.A. Srar,; K.-S. Chung and A. Mansour, "Adaptive Array Beamforming Using a Combined LMS-LMS Algorithm", IEEE Transactions on Antennas and Propagation, Vol.58 , pp. 3545 - 3557, 2010.

[7] J. Freudenberger and S. Stenzel, "Suppression of Engine Noise Harmonics Using Cascaded LMS Filters", Proceedings of the 10. ITG Symposium on Speech Communication; pp. 1-4, Braunschweig, Germany, September 2012.

[8] W. Orozco and H. Pérez, "Beamforming based on Constrained Linear Estimation: Analysis and Simulations", XIII Congreso Nacional de Ingeniería Electromecánica y de Sistemas, México DF, November 2012.

[9] A. H. Sayed, Fundamentals of Adaptive Filtering, Jhon Wiley & Sons, Inc., Hoboken, New Jersey, 2003, pp. 128-130.

[10] M. Arezk and D. Berkani, "Fast Algorithms with Low Complexity for Adaptive Filtering",WSEAS Transactions on Signal Processing Vol. 5, pp. 23-31, 2009.

[11] J. D. Kraus and R. J. Marhefka, Antennas For All Applications, McGrawHill, New York, 2002, pp. 109-120.

[12] B. Widrow and S. D. Stearns, Adaptive Signal Processing, Prentice-Hall, New Jersey, 1985, pp. 26.

[13] S. Haykin, Adaptive Filter Theory, Prentice-Hall, New Jersey, 1986, pp. 197–201.

[14] B. Widrow, "Adaptive filters I: Fundamental", Stanford Electronics Labs., Stanford, Calif., Rept. SEL-66-126 (Tech. Rept. 6765-6), December 1966.

Walter Orozco Tupacyupanqui was born in Cuenca, Ecuador, on December 13, 1976. He received the B.Sc. degree in Electrical Engineering from University of Cuenca, Cuenca, Ecuador, in 2002 and the M.Sc. degree in Electrical and Computer Engineering from New York Institute of Technology, Old Westbury, USA, in 2005 with academic distinction. Since January 2012, he has been enrolled in the graduate Ph.D. program in Communications and Electronic at The Mechanical and Electrical Engineering School, Culhuacan Campus, National Polytechnic Institute of Mexico. From March 2006 to October 2008 he was with the Electrical Engineering Department at University of Cuenca where he was a Professor. In September 2006, he joined the Electrical and Electronic Engineering Department at Salesian Polytechnic University where he is currently a Professor. From July 2009 to February 2009, he was Director of the Master Programme in Electrical Power Systems at University of Cuenca. He is a member of the IEEE. His principal research interests are adaptive systems, signal processing, control systems, communications systems and related fields.

Mariko Nakano-Miyatake received the M.E. degree in Electrical Engineering from the University of Electro-Communications, Tokyo Japan in 1985, and her Ph. D in Electrical Engineering from The Universidad Autonoma Metropolitana (UAM), Mexico City, in 1998. From July 1992 to February 1997 she was a Department of Electrical Engineering of the UAM Mexico. In February 1997, she joined the Graduate Department of The Mechanical and Electrical Engineering School of The National Polytechnic Institute of Mexico, where she is now a Professor. Her research interests are in information security, image processing, pattern recognition and related field. Dr. Nakano is a member of the IEEE, RISP and the National Researchers System of Mexico.

Hector Perez-Meana received his M.S: Degree on Electrical Engineering from the Electro-Communications University of Tokyo Japan in 1986 and his Ph.D. degree in Electrical Engineering from the Tokyo Institute of Technology, Tokyo, Japan, in 1989. From March 1989 to September 1991, he was a visiting researcher at Fujitsu Laboratories Ltd, Kawasaki, Japan. From September 1991 to February 1997 he was with the Electrical Engineering Department of the Metropolitan University of Mexico City where he was a Professor. In February 1997, he joined the Graduate Studies and Research Section of The Mechanical and Electrical Engineering School, Culhuacan Campus, of the National Polytechnic Institute of Mexico where he was the Dean from August 2006 to December 2009. In 1991 he received the IEICE excellent Paper Award, and in 2000 the IPN Research Award and the IPN Research Diploma. In 1998 he was Co-Chair of the ISITA'98, and in 2009 he was the General Chair of The IEEE Midwest Symposium on Circuit and Systems (MWSCAS). Prof. Perez-Meana has published more that 100 papers and two books. He also has directed 15 PhD theses and more than 30 Master theses. He is a senior member of the IEEE, member of The IEICE, The Mexican Researcher System and The Mexican Academy of Science. His principal research interests are adaptive systems, image processing, pattern recognition, watermarking and related fields.